Modelling tidal energy extraction in a depth-averaged coastal domain

Modelling Tidal Energy Extraction in a Depth-Averaged Coastal Domain

S. Draper, G.T. Houlsby, M.L.G. Oldfield and A.G.L. Borthwick

Department of Engineering Science,
University of Oxford,
Parks Road, Oxford, OX1 3PJ, UK

Abstract

An extension of actuator disc theory is used to describe the properties of a tidal energy device, or row of tidal energy devices, within a depth-averaged numerical model. This approach allows a direct link to be made between an actual tidal device and its equivalent momentum sink in a depth-averaged domain. Extended actuator disc theory also leads to a measure of efficiency for an energy device in a tidal stream of finite Froude number, where efficiency is defined as the ratio of power extracted by one or more tidal devices to the total power removed from the tidal stream. To demonstrate the use of actuator disc theory in a depth-averaged model, tidal flow in a simple tidal channel is approximated using the shallow water equations and the results compared with published analytical solutions.

1 Introduction

The deployment of a large-scale tidal farm will influence the hydrodynamics within a coastal basin. To understand this influence, recent studies have considered analytical models of tidal power extraction from channels (see, for example [1, 2, 3, 4]), numerical models of site specific coastal regions (see, for example [5, 6, 7]) and numerical models of general coastal regions [8, 9]. These studies have typically considered the maximum power that can be extracted from a coastal site and the impact of tidal devices on tidal variables such as the local tidal range and tidal current. As a result, a reasonably complete understanding has been developed of the power potential of well-bounded tidal streams, such as tidal flow through a single channel between two basins [1, 2, 3]. However, a growing number of less well-bounded sites have been identified as having potentially significant tidal energy resources (see, for example [10, 11]).

Fig. 1 sketches a set of idealised geometries that summarise the different generic types of coastal sites that might be encountered in practice. This basis set defines four coastal geometries: a) a channel between two disconnected basins; b) a coastal inlet, estuary or bay; c) a headland; and, d) an island located near a much larger land mass. Noting that the hydrodynamic behaviour of the geometry depicted in Fig. 1(a) has received considerable attention to date [1, 2, 3], a detailed understanding of the power potential and hydrodynamic effects of energy extraction in the remaining geometries would provide an ideal reference point for tidal resource assessment.

Numerical simulations offer a useful means of predicting how less well-bounded coastal sites, such as those depicted in Figs 1(c) and 1(d), react to tidal power extraction. Previous numerical models have all been based on approximations to the Shallow Water Equations (SWEs), with the effects of tidal devices typically

introduced through an added roughness or a general source term [5, 6]. Although added roughness can represent tidal devices to a first order approximation, it is difficult to relate the roughness value to a particular tidal device configuration. Attempts to do so have been empirical and have not yet been verified [7]. In the present paper we use actuator disc theory to describe a tidal device within a depth-averaged numerical model, following Garrett and Cummins who used a similar approach within a 1D analytical model [12]. A key advantage of actuator disc theory is that it provides a theoretical argument that links a tidal device, defined by a blockage ratio and porosity (see Section 3 for definitions), to the equivalent momentum sink that the device should impart within a depth-averaged domain. Furthermore, simple scaling arguments suggest that actuator disc theory might also provide a useful approach for unbounded flows.

The layout of the paper is as follows. Section 2 reviews the literature on analytical and numerical modelling of tidal power extraction. Section 3 presents an extension to the actuator disc model of Whelan et al. [13] that accounts for downstream mixing. The extended model is used to investigate the efficiency of a tidal device in a tidal stream of finite Froude number. Using simple scaling assumptions, it is argued in Section 4 that actuator disc theory can provide a useful description of tidal power extraction in coastal basins driven by long waves. In Section 5 the SWEs are outlined and the numerical boundary condition for a line of tidal devices is discussed. Section 6 presents results obtained for a simple tidal channel between two basins including power extraction. The numerical results are compared with an analytical model due to Garrett and Cummins [1].

2 Literature Review

1.1 One-Dimensional Theoretical Models

The following one-dimensional (1D) theoretical models have been developed to describe energy extraction from a channel. The first, due to Garrett and Cummins [1], investigates a channel connecting two large basins or oceans, whose tides differ in phase and/or amplitude. Such a model might, for instance, represent a first approximation to the Pentland Firth, between Scotland and the Orkney Islands. The geometry therefore resembles Fig. 1(a), or, if the island is large, Fig. 1(d). The second theoretical model, due to Garrett and Cummins [2] and Blanchfield et al. [3], concerns a channel connecting a large basin or ocean to an enclosed basin or bay. This model is a generalised form of Fig. 1(a) if the two large basins are only connected through the channel. It is also a compact case of Fig. 1(b), since the bay dimensions are assumed small in comparison to the tidal wavelength. Both of the theories adopt the 1D SWEs and make several simplifying assumptions which are discussed in detail by Garrett and Cummins [14]. Based on these assumptions the maximum average power $\overline{P}$ that can be extracted from the channel when subjected to a sinusoidal driving tide of amplitude a, is shown to be

$$\overline{P} = \gamma \rho g a Q_{\max}, \tag{1}$$

where $Q_{\max}$ is the maximum flow rate in the undisturbed channel, ρ is the density, g is acceleration due to gravity and γ is a dimensionless factor that varies between 0.19 and 0.26. The range of γ is representative of the dynamic balance in the channel, with a value of 0.21 in both models indicating that the flow is dominated by quadratic drag losses as opposed to acceleration effects [1, 3]. However, since the range of γ is small, taking $\gamma = 0.22$ provides a useful approximation to both regimes [1, 14]. The

maximum average power is then defined in terms of the undisturbed flow rate and the driving amplitude, both of which can be measured from observations and numerical simulations [1, 5, 14]. As a result Eq. (1) provides a useful prediction of power potential that is accurate to the leading order, provided the exit separation and other non-linear losses vary with the flow rate squared as tidal devices are introduced [14].

The analytical models also provide an indication of hydrodynamic effects. For instance, at optimum power extraction the flow rate through a channel between two large basins is reduced to 58% if drag forces are dominant in the undisturbed state [1]. However if, for example, a 10% reduction in the flow rate is considered 44% of maximum average power can still be achieved (when $\gamma = 0.21$) [5]. For the second model, a similar trend is noted [6, 15].

Garrett and Cummins [12] have suggested a way of extending 1D theory to channels partially blocked by tidal devices, using linear momentum actuator disc theory (LMADT) in the region containing the devices. Although actuator disc theory ties in well with the assumptions of the 1D theoretical models, it also requires further assumptions in the vicinity of the power extraction device, including constant channel width, uniform along channel bathymetry, uniform upstream flow, and steady state conditions.

1.2 Numerical Simulations

Several site-specific numerical simulations have been documented. Amongst these are studies of the Minas Passage by Karsten et al. [6], the Johnstone Strait by Sutherland et al. [5] and the Portland Bill by Blunden and Bahaj [7, 16]. In each of these studies, the presence of tidal devices is modelled by an additional bed friction source term which varies according to the square of the local tidal current velocity. For example, in both [5] and [6] the friction coefficient is defined as

$$C_d = k_o + k_t, \tag{2}$$

where k_o is related to natural friction and k_t represents tidal turbines. Since the objective of [5] and [6] was to investigate the maximum extractible power, no particular physical description of k_t is discussed. In [7, 16] the coefficient was assigned based on a case study of a yawed horizontal axis marine current turbine and a hypothetical array design.

Bryden and Couch [8] and Polagye et al. [9] have studied general coastal basins using shallow flow numerical models. Bryden and Couch considered flow around an island with turbines idealised as added roughness. Polagye et al. simulated uniform flow in a channel with one open boundary, one closed boundary and two discontinuous changes in width that define an internal extraction zone. The tidal devices were represented as line discontinuities across the complete width of the power extraction zone.

3 Momentum Actuator Disc Theory

The linear momentum actuator disc theory (LMADT) presented by Garrett and Cummins [12] considers an actuator disc in a flow of constant cross section, bounded by parallel channel walls and a constant free surface profile. Recently Whelan et al. [13] applied LMADT to provide an approximation to the flow field around an actuator disc in an open channel flow with a non uniform free surface. Houlsby et al. [17] extend Whelan et al.'s theory to include downstream mixing and hence provide a local steady state description of a real turbine, or line of turbines, that can be introduced as a perturbation in both velocity and depth into a depth averaged numerical model. We provide a summary of that approach here.

Fig. 2 illustrates a one dimensional channel containing an actuator disc with associated downstream mixing. It is assumed that the upstream conditions are uniform with constant velocity u and depth h. The channel, or centre to centre spacing between adjacent turbines, has constant width b. The flow is inviscid. At Stations 1, 4 and 5 in Fig. 2 it is assumed that the pressure is hydrostatic and the flow is uniform. The velocity $u_{b4} = \beta_4 u$ denotes the bypass flow velocity at Station 4, while $u_{t2} = \alpha_2 u$ and $u_{t4} = \alpha_4 u$ define the turbine flow velocity at Stations 2 and 4 respectively. The thrust T is the horizontal force applied to the fluid from the turbine. The turbine(s), idealised as actuator discs, occupy an area A, and so a dimensionless blockage ratio may therefore be defined as $B = A/(hb)$. The analysis which follows is indifferent to the location or shape of the actuator disc in the effective cross section hb.

Following Whelan et al. [13], applying continuity, and energy and momentum conservation selectively between Stations 1 and 4 leads to a quartic equation describing the bypass velocity

$$\frac{Fr^2}{2}\beta_4^4 + 2\alpha_4 Fr^2\beta_4^3 - \left(2 - 2B + Fr^2\right)\beta_4^2 - \left(4\alpha_4 + 2\alpha_4 Fr^2 - 4\right)\beta_4 + \left(\frac{Fr^2}{2} + 4\alpha_4 - 2B\alpha_4^2 - 2\right) = 0, \tag{3}$$

where $Fr = u/\sqrt{gh}$ is the upstream Froude number. Provided that the upstream Froude number is known and the turbine is defined by a blockage ratio and the velocity coefficient α_4, equation (3) can be solved for β_4. Applying the Bernoulli equation and continuity in the bypass flow then allows for the calculation of the remaining velocity coefficient α_2

$$\alpha_2 = \frac{\alpha_4(\beta_4 - 1)}{B(\beta_4 - \alpha_4)}\left[1 - \frac{Fr^2}{2}(\beta_4 + 1)\right]. \tag{4}$$

Alternatively, the turbine could be defined by a blockage ratio and an induction factor $a = 1 - \alpha_2$, in which case equations (3) and (4) are solved simultaneously for β_4 and α_4. In general any three independent parameters are sufficient to define the flow field provided that the bypass flow does not become critical (where the relevant physical root of (3) becomes complex [17]). The power and thrust can be determined in terms of a power coefficient C_P and a thrust coefficient C_T

$$T = \frac{1}{2}\rho u^2 Bbh\left(\beta_4^2 - \alpha_4^2\right) = C_T\frac{1}{2}\rho u^2 Bbh, \tag{5a}$$

and

$$P = \alpha_2 uT = \frac{1}{2}\rho u^3 Bbh\alpha_2\left(\beta_4^2 - \alpha_4^2\right) = C_P\frac{1}{2}\rho u^3 Bbh. \tag{5b}$$

Since the flow is not uniform with depth at Station 4, we assume that downstream mixing will occur. Applying momentum conservation in the horizontal direction between Stations 1 to 5 then leads to

$$\frac{1}{2}\rho g b\left(h^2-(h-\Delta h)^2\right)-T=\rho b h u\left(\frac{uh}{h-\Delta h}-u\right). \tag{6}$$

Substituting for the thrust coefficient and rearranging then gives

$$\frac{1}{2}\left(\frac{\Delta h}{h}\right)^3-\frac{3}{2}\left(\frac{\Delta h}{h}\right)^2+\left(1-Fr^2+\frac{C_T B Fr^2}{2}\right)\frac{\Delta h}{h}-\frac{C_T B Fr^2}{2}=0. \tag{7}$$

This is a cubic expression that can be solved for the downstream depth change $\Delta h = h - h_5$. Notably for zero Froude number the relative depth change tends to the solutions $\Delta h/h \to 0$, 1, and 2, with the former being the physically admissible solution. We determine the power lost in the wake in terms of Δh from

$$P_W=\frac{1}{2}\rho u^3 B b h \alpha_2 \alpha_4^2+\frac{1}{2}\rho u^3 b h(1-B\alpha_2)\beta_4^2-\frac{1}{2}\rho u^3 b h\left(\frac{h}{h-\Delta h}\right)^2+h b u\left(h_4-h_5\right)\rho g \tag{8}$$

Combining (8) with (5b) gives the total power lost in the channel

$$P+P_W=\rho g u b h \Delta h\left(1-Fr^2\,\frac{1-\Delta h/(2h)}{(1-\Delta h/h)^2}\right), \tag{9}$$

and a measure of efficiency, defined as the ratio of power extracted by the tidal device(s) to the total power removed from the tidal stream, follows directly as,

$$\eta=\frac{P}{P+P_W}=\frac{P}{\rho g u b h \Delta h}\left(1-Fr^2\,\frac{1-\Delta h/(2h)}{(1-\Delta h/h)^2}\right)^{-1}. \tag{10}$$

We can make several observations about this measure of efficiency and its design implications for tidal turbines. Firstly, as $Fr \to 0$, $\eta \to \alpha_2$, which agrees with the

result discussed by Garrett and Cummins [12] for an actuator disc in a constrained volume flow. This result is easy to deduce from (10) by ignoring the term proportional to Fr^2, noting that the power can be written as $P=(\alpha_2 u)T$, and rearranging $u\times(6)$ to give

$$uT = \rho g u b h\left(\Delta h - \frac{\Delta h}{2}\frac{\Delta h}{h} - Fr^2\frac{h\Delta h}{h-\Delta h}\right), \tag{11}$$

Ignoring terms proportional to Fr^2 and $\Delta h/h$ (since $\Delta h/h \to 0$ when $Fr \to 0$ from (7)), we have $\rho g u b h \Delta h \to uT$ and so $\eta \to \alpha_2$ as required.

For arbitrary Froude number, the effect of the free surface on efficiency is best appreciated through manipulation of (10). Combining (10) with the expression for power from (5b) and substituting for $C_T B Fr^2/2$ from (7) leads to

$$\eta = \alpha_2\frac{(1-\Delta h/(2h)) - Fr^2(1-\Delta h/h)^{-1}}{1-Fr^2(1-\Delta h/(2h))(1-\Delta h/h)^{-2}}. \tag{12}$$

For small but finite Froude number and downstream depth change (so that $Fr^2(1-\Delta h/h)^{-1} << 1$), which is often realistic for tidal flows, the efficiency can be written as

$$\eta \approx \alpha_2\left(1-\frac{1}{2}\frac{\Delta h}{h}\right). \tag{13}$$

This indicates that the main effect of the non-zero Froude number and associated relative depth change, is to reduce efficiency by a factor of $(1-\frac{1}{2}\Delta h/h)$, as compared to a device with a depth change that is negligible compared to upstream depth.

The measure of efficiency defined by (12) is maximised when $\alpha_2 \to 1$ and $\Delta h/h \to 0$. However this only applies when no power is extracted from the flow. Based on this result it is tempting to abandon efficiency as a primary optimisation

parameter. However, an interesting problem arises if we restrict the downstream depth change, possibly for environmental reasons, or restrict the total amount of power that can be removed from the channel, and then optimize efficiency. For a given Froude number and downstream depth change, it then follows directly from (13) that increasing α_2 will improve efficiency. An equivalent conclusion is that efficiency increases with blockage ratio, since the blockage ratio increases monotonically with α_2 when the Froude number and depth change are fixed (see Fig. 3). Of course there is a limit to how close to unity α_2 and B can become to extract the required depth change. Using the theory described here the bypass flow becomes critical when α_2 and B are too large (see Fig. 3).

Efficiency can also be improved by increasing the number of turbine fences that in combination lead to an overall fixed downstream depth change. This gain is achieved because, as the number of fences increases, the incremental depth change across each fence reduces, causing the incremental efficiency to rise according to (13). In addition, α_2 is a decreasing function of the downstream depth change, which leads to a further gain in incremental efficiency from (13). In fact, since α_2 is strongly dependent on the incremental depth change, and insensitive to the small increase in Froude number and blockage ratio between successive fences, the optimum distribution of depth change across a series of fences is very close to a simple average. Fig. 4 shows the net efficiency for a channel of numerous turbine fences, each extracting an equal proportion of the total downstream depth change and positioned in series so that complete mixing occurs between successive turbines. It is interesting to observe from Fig. 4 that extraction of a fixed amount of power from a flow at higher

Froude number can be more efficient, for a given number of turbine rows, because a larger α_2 is permissible.

4 Use of Actuator Disc Theory in a Depth-Averaged Dynamic Model

We now discuss how a row of turbines might be defined in a 2D depth-averaged numerical model using LMADT. Fig. 5 illustrates two typical scenarios for a row of turbines. Fig. 5(a) depicts a fence that extends completely across a channel. Here flow passes through the fence and mixes to form a smooth mean vertical velocity profile over a length l_v, which from available experimental evidence may be roughly of the order of 20 tidal device diameters [18] (or perhaps 200-300 m for a 10-15 m diameter axial flow turbine). Within this mixing region (denoted by the shaded region in Fig. 5(a)) the flow structure will be highly three dimensional as the faster bypass flow mixes vigorously with the slower turbine flow. In experiments on porous disks this mixing process has been shown to be dependent on the ambient turbulence in the tidal stream and the proximity of the tidal device to the seabed and free surface [18]. Additional dependence on turbulence introduced by the tidal device, the tidal device size, blockage and shape, and seabed friction is expected.

Due to the periodicity of the turbine placement in the fence shown in Fig. 5(a), and because l_v is much smaller than a tidal wavelength so that the flow is essentially quasi-steady, it is reasonable to assume that the perturbation to the free surface and depth-averaged velocity at each discrete location along the fence can be approximated well by Equation (7) when the blockage ratio is calculated taking b to be the centre to centre spacing between turbines. Furthermore, since l_v is also smaller than the typical mesh discretisation in a 2D depth-averaged model (of the order of kilometres), introducing this momentum sink as a line discontinuity, indicated in Fig. 5 and discussed further in Section 5, offers a useful approach to account for the tidal devices in a 2D depth-averaged model.

Fig. 5(b) illustrates a fence of turbines in an unbounded 2D flow. The flow field about this fence can be split into two fields: (1) the near field extending over the distance l_v and (2) a far field extending over a distance l_h that will be dependent on the extent of the tidal fence and so will generally be much larger than l_v.

Within the near field the flow structure is expected to be similar to that in Fig. 5(a). In the far field region behind the fence ($x >> l_v$ in Fig. 5) the extraction of momentum at the fence will lead to a depth-averaged wake with velocity lower than that in the surrounding tidal stream. Generally, actuator disc theory cannot be used to describe the energy extraction of the entire fence over this length scale because the upstream flow may not be uniform, there might be substantial bed roughness and changes in bathymetry, or the length scale may be too large to validate the assumption of steady flow.

However, we propose that LMADT can be used in the near field to determine the momentum sink imparted by the turbines within the fence. This amounts again to the assumption that a turbine within the fence has a blockage ratio that is calculated based on the centre to centre spacing between turbines.

By analogy to experiments on a line of diffusers [20, 21] and similar flow structures in shallow flows [19], the mixing of the far field will result from shear generated turbulence, and will be dependent on the bed roughness, bathymetry and, as mentioned above, the length of the fence. These parameters will typically vary between different locations and can be accounted for reasonably well in the depth-averaged numerical model.

5 Numerical Modelling

To provide insight into the physical relationships that govern shallow flow hydrodynamics in a coastal basin the SWEs are commonly adopted:

$$\frac{\partial h}{\partial t} + \frac{\partial (uh)}{\partial x} + \frac{\partial (vh)}{\partial y} = 0, \tag{14a}$$

$$\frac{\partial (uh)}{\partial t} + \frac{\partial \left(u^2 h\right)}{\partial x} + \frac{\partial (uvh)}{\partial y} = -gh\frac{\partial \zeta}{\partial x} - \frac{\tau_x}{\rho} + fvh, \tag{14b}$$

and

$$\frac{\partial (vh)}{\partial t} + \frac{\partial (uvh)}{\partial x} + \frac{\partial \left(v^2 h\right)}{\partial y} = -gh\frac{\partial \zeta}{\partial y} - \frac{\tau_y}{\rho} - fuh, \tag{14c}$$

where x and y are spatial coordinates, h is the total water depth, ζ is the free surface elevation above the mean water depth, u and v are the horizontal depth-averaged velocity components, g is the acceleration due to gravity, ρ is fluid density, t is time, f is the Coriolis parameter and, τ_x and τ_y are frictional shear stress terms due to bed friction

$$\tau_x = \rho C_d u|\mathbf{u}| \quad \text{and} \quad \tau_y = \rho C_d v|\mathbf{u}|, \tag{15}$$

where $|\mathbf{u}| = \sqrt{u^2 + v^2}$ and C_d is a drag coefficient.

In the present work, the SWEs given by (14) are solved using the discontinuous Galerkin finite element method (see [20, 21] for a general description of this method). The model commences from quiescent initial conditions. With reference to Fig 1(b), three boundary conditions are implemented. Tidal forcing is imposed at the open boundary Γ_o, such that

$$h(x, y, t) = h_o(x, y) + \sum a_i \cos(\omega_i t + \varphi_i), \text{ on } \Gamma_o, \tag{16}$$

where $h_o(x, y)$ is the mean water depth along the open ocean boundary, and a_i is the amplitude, ω_i is the frequency and φ_i is the phase of the ith tidal constituent. At the coastline Γ_c a reflective boundary condition is implied, such that

$$\mathbf{u}.\mathbf{n} = 0, \quad \text{on } \Gamma_c. \tag{17}$$

The third boundary condition represents the fence of tidal devices as a line discontinuity, whereby

$$\frac{\Delta h}{h} = G(Fr, B, \alpha_4), \text{ on } \Gamma_t \tag{18}$$

where $\Delta h/h$ is, as in Section 3, the relative depth change across the tidal devices. Condition (18) is acceptable provided the length scale of the wake behind the turbine array is much smaller than the mesh size [9]. (This approach is also consistent with observations for a line of diffusers, each with diameter smaller than the water depth, discharging into shallow water. Considerable success has been achieved numerically and analytically in treating diffusers as a line source of momentum in a depth-averaged framework [22, 23].) To understand how the discontinuity is implemented in a finite volume or discontinuous Galerkin finite element scheme, consider two adjacent finite volumes, V_1 and V_2, separated by a fence of tidal turbines. Values for h_1, u_{n1}, h_2 and u_{n2} (where the subscript n refers to the component in the direction of the unit normal vector directed out of the finite volume V_1) are determined either side of the interface between V_1 and V_2 by interpolation from the discrete solution of the SWEs. Modified interface fluxes $F\left(h_1^*, u_{n1}^*, v_t^*\right)$ and $F\left(h_2^*, -u_{n2}^*, v_t^*\right)$ are then calculated for each finite volume, using the tidal device properties and the characteristic invariants. The four equations defining the unknowns h_1^*, u_{n1}^*, h_2^* and u_{n2}^* are

$$u_{n1} + 2\sqrt{gh_1} = u_{n1}^* + 2\sqrt{gh_1^*}, \tag{19a}$$

$$u_{n2} - 2\sqrt{gh_2} = u_{n2}^* - 2\sqrt{gh_2^*}, \tag{19b}$$

$$h_1^* u_{n1}^* = h_2^* u_{n2}^*, \tag{19c}$$

and

$$\frac{\Delta h^*}{h} = \text{sign}(u_{n1})\left(h_1^* - h_2^*\right) / \max(h_1, h_2) = G(Fr, B, \alpha_4), \tag{19d}$$

where G characterises the tidal devices. Using LMADT, G is given by (7) thereby defining the dimensionless depth change implicitly for a given Froude number, blockage ratio, and wake induction factor. The Froude number is a function of the upstream depth and velocity chosen appropriately from h_1, u_{n1}, h_2 and u_{n2}.

There is no direct adjustment required for the tangential velocity components v_{t1} and v_{t2} (where the subscript t refers to the tangential component directed anti-clockwise around V_1) because it is assumed that the devices will not exert a force in the tangential direction. This is consistent with the classical actuator disc analysis. The tangential velocity used to compute the numerical flux v_t^* is determined relative to the contact wave speed as defined in the HLLC method [24].

6 A Simple Channel

Fig. 6 depicts the computational mesh used to represent a simple channel between two large basins. A series of simulations was undertaken to examine the idealisation of the turbines in the present numerical model (as discussed in Section 5), and to compare the predictions with solutions obtained from the first theoretical model due to Garrett and Cummins [2], discussed in Section 2.

Fig. 6 shows the reference geometry considered, which has an aspect (breadth to length) ratio of $W/L = 0.4$. Simulations were also carried out for $W/L = 0.1$ and 0.2. In all cases, the bathymetry was uniform and the bed friction coefficient C_d was kept spatially constant for each test, taking the values indicated in Table 1. To simulate a tidal stream through the channel, the left open boundary of the domain, located a distance of $10L$ from the channel, was driven by a single sinusoidal constituent, with amplitude varying around the perimeter to simulate a plane incident and reflected linear wave propagating parallel to the channel direction. The depth at the right open boundary was kept constant. The maximum average available power was explored over the parameter range given in Table 1. In all tests the mean depth was 70 m and $L = 10\,000$ m. Coriolis terms were ignored and the amplitude of the driving tide was adjusted to ensure that the Froude number ($Fr \sim 0.05 - 0.20$) was realistic in the undisturbed channel for a tidal energy site. Tests 5 and 6 represent steady state simulations representative of a quasi-steady flow.

For each test, the sinusoidal boundary condition was not changed as more turbines were introduced. The boundary therefore had zero impedance, which could be physically interpreted as a very deep and abrupt continental shelf [25].

	W/L	ω	C_d	a/h_o	Fr
Test 1	0.4	0.00014	0.035	0.040	0.102
Test 2	0.4	0.00014	0.0035	0.015	0.169
Test 3	0.4	0.00014	0.0105	0.015	0.104
Test 4	0.4	0.00014	0.00105	0.008	0.089
Test 5	0.4	0	0.035	0.113	0.163
Test 6	0.4	0	0.0105	0.034	0.163

Table 1: Parameter range considered for the simple channel. The Froude number represents the simulated value at the centre of the channel when no tidal devices are present.

Fig. 7 shows the power extracted from the channel as a function of the channel flow rate for various tidal device fence blockage ratios. In each case, the devices are placed across the centre of the channel (see Fig. 6) and the wake induction factor is taken to be $\alpha_4 = 1/3$, which is close to optimum local power extraction. The power displayed in Fig.7 is normalised against the predicted maximum average power calculated from (1) using $\gamma = 0.22$ ($\gamma = 0.21$ for the quasi-steady tests 5 and 6), the driving tidal amplitude, and the simulated flow rate when the blockage ratio is zero. The flow rate is normalised against the simulated flow rate when the blockage ratio is zero. It is clear from Fig. 7 that there is an optimal blockage ratio for power extraction. Furthermore the normalised optimum power appears to be close to unity for all tests indicating satisfactory agreement with the analytical model of Garrett and Cummins [1]. In general, the numerical and analytical results are unlikely to be identical for atleast three reasons: (1) The value of $\gamma = 0.22$ is only an approximation to the dynamics in the channel and in general will be too large for shallow channels with high natural friction (high C_d) and too small for deep channels with low natural friction (small C_d) [1]; (2) the analytical model assumes that the turbines experience a drag that is quadratic with flow rate, whereas the LMADT defined in Section 3, and used numerically to define the turbines, does not experience drag that is quadratic

with flow rate if the Froude number is large; and (3) the 2D numerical model includes separation losses and other non-linear losses that may not vary with the flow rate squared.

To investigate the last of these reasons Fig. 8 displays velocity contours along the channel for low and high blockage ratio for one particular test case. It is clear that the velocity fields are almost self-similar despite the addition of turbines. Consequently, separation losses from the channel, which are generally quadratic with the flow velocity, are simulated as quadratic in the flow rate as more turbines are added (since the exit cross sectional area is unchanged). This, in part, ensures that the agreement between the analytical theory and the numerical results is satisfactory.

Lastly, in Fig. 7 it is clear that a lower blockage ratio is required to reach maximum power when friction drag is small. This result is predicted by the theory [1] and discussion in [14] where, for a small Froude number, the optimal blockage ratio is noted to be an increasing function of friction losses. In the case of separation losses, but no friction losses, the smallest optimal blockage ratio is given as approximately 0.46, provided the channel area at the location of the turbines is equal to the channel area at the exit [14]. For the channel geometry in Fig. 6 it is clear that the exit area should be greater than the channel area at the turbines, and so this lower bound reduces slightly. For all the tests in Fig. 7 the optimal blockage ratio is above 0.46, but not by a significant amount. The important conclusion therefore, as noted in [14], is that the optimal blockage can be achieved with only one row, or fence, of devices.

6 Conclusions

Existing 1D theoretical models provide a reasonably complete explanation of the physics of tidal energy extraction from channels. Numerical 2D simulations are useful for channels that do not vary smoothly in geometry and for channels with asymmetrically placed turbine fences that partially block the flow. There is also considerable scope to better understand unbounded flows and the power potential of the scenarios sketched in Fig. 1(c) and (d). Extending LMADT to account for both a deforming free surface and downstream mixing provides an efficiency measure for a tidal device(s) in a uniform tidal stream. Given a constraint on the amount of power that can be extracted from the flow, then large turbines and many rows of turbines are most efficient. In practice upper limits have to be imposed on both of these parameters, both for serviceability requirements and economic reasons. LMADT provides a theoretical means of introducing a line, or fence, of tidal turbines into a depth-averaged numerical model. A numerical model based on the SWEs has been shown to produce results that are consistent with existing analytical models. This numerical approach is being extended to unbounded tidal flows, typical of those in Fig. 1(c) and (d), and further testing and validation is planned.

7 Acknowledgements

The first author acknowledges the kind support of the Rhodes Trust. Reviewers comments are also gratefully acknowledged.

8 References

[1] C. Garrett and P. Cummins. 'The power potential of tidal currents in channels', Proc. R. Soc. Lond A, 2005, **461**, pp. 2563-2572

[2] C. Garrett and P. Cummins. 'Generating Power from Tidal Currents', J. Waterway, Port, Coastal and Ocean Engineering, 2004, **130**, pp. 114-118

[3] J. Blanchfield, C. Garrett, P. Wild and A. Rowe. 'The extractable power from a channel linking a bay to the open ocean', Proc. IMechE Part A: J. Power and Energy, 2008, **222**, pp. 289-297

[4] I. G. Bryden and S.G. Couch. 'How much energy can be extracted from moving water with a free surface: A question of importance in the field of tidal current energy', Renewable Energy, 2007, **32**, pp. 1961-1966

[5] G. Sutherland, M. Foreman and C. Garrett. 'Tidal current energy assessment for Johnstone Strait, Vancouver Island', Proc. IMechE Part A: J. Power and Energy, 2007, **221**, pp. 147-157

[6] R.H. Karsten, J.M. McMillan, M.J. Lickley and R.D. Haynes. 'Assessment of tidal current energy in the Minas Passage, Bay of Fundy', Proc. IMechE Part A: J. Power and Energy, 2008, **222**, pp. 493-507

[7] L.S. Blunden and A.S. Bahaj. 'Initial evaluation of tidal stream energy resources at Portland Bill, UK', Renewable Energy, 2006, **31**, pp. 121-132

[8] I. G. Bryden, S. J. Couch, A. Owen and G. Melville. 'Tidal current resource assessment', Proc. IMechE Part A: J. Power and Energy, 2007, **221**, pp. 125-135

[9] B. Polagye, P. Malte, M.Kawase and D. Durran. 'Effect of large-scale kinetic power extraction on time-dependent estuaries', Proc. IMechE Part A: J. Power and Energy, **222**, pp. 471-484

[10] Black and Veatch. 'Phase II: UK Tidal Stream Energy Resource Assessment', Carbon Trust Marine Energy Challenge, 2005

[11] R. Bedard, M. Previsic, G. Hagerman, B. Polagye, W. Musial, J. Klure, A. V. Jouanne, U. Mathur, C. Collar, C. Hopper, S. Amsden. 'North American Ocean Energy Status- March 2007', Proc. 7th EWTEC, Porto, Portugal, 2007

[12] C. Garrett and P. Cummins. 'The efficiency of a turbine in a tidal channel.' J. Fluid Mechanics, 2007, **588**, pp. 243-251

[13] J.I. Whelan, J.M. Graham and J.Peiro. 'A free-surface and blockage correction for tidal turbines', J. Fluid Mechanics, 2009, **624**, pp. 281-291

[14] C. Garrett and P.Cummins. 'Limits to tidal current power', Renewable Energy, 2008, **33**, pp. 2485-2490

[15] J. Blanchfield, C. Garrett, P. Wild and A. Rowe. 'Tidal stream power resource assessment for Masset Sound, Haida Gwaii', Proc. IMechE Part A: J. Power and Energy, 2008, **222**, pp. 485-492

[16] L.S. Blunden and A.S. Bahaj. 'Effects of tidal energy extraction at Portland Bill, southern UK predicted from a numerical model'. Proc. 7th EWTEC, Porto, Portugal, 2007

[17] G.T. Houlsby, S. Draper and M.L.G. Oldfield. 'Application of Linear Momentum Actuator Disc Theory to Open Channel Flow', 2008, Technical Report 2296-08, OUEL

[18] L.E. Myers and A.S. Bahaj. 'Experimental analysis of the flow field around horizontal axis tidal turbines by use of scale mesh disk rotor simulators.' Ocean Engineering, 2010, **37**, pp. 218-227

[19] G.H. Jirka. 'Large scale flow structures and mixing processes in shallow flows'. J. Hydraulic Research, 2002, **39**, pp. 567-573

[20] C. Eskilsson and S.J. Sherwin. 'A triangular spectral/hp discontinuous Galerkin method for modelling the 2D shallow water equations', Int. J. Numerical Methods, 2004, **45**, pp. 605-623.

[21] F. X. Giraldo and T. Warburton. 'A high-order triangular discontinuous Galerkin oceanic shallow water model', International Journal for Numerical Methods, 2008, **56**, pp. 899-925

[22] J. H. Lee and M. D. Greenberg. 'Line momentum source in shallow inviscid fluid', J. Fluid Mechanics. 1984, **145**, pp. 287-304

[23] J. H. Lee and G. H. Jirka. 'Multiport diffuser as a line source of momentum in shallow water', Water Resources Research, 1980, **16**, pp. 695-708

[24] E.F. Toro, M. Spruce and W. Speares. 'Restoration of the contact surface in the HLL-Reimann solver', Shock Waves, 1994, **4**, pp. 25-34.

[25] C. Garrett and D. Greenberg. 'Predicting changes in tidal regime: the open boundary problem', J. Physical Oceanography, 1977, **7**, pp. 171-181

Nomenclature

A = Area of a turbine(s)
a = Amplitude of a tidal constituent
B = Blockage ratio
b = Uniform channel width
C = Dimensionless coefficient
$F(\ )$ = Numerical flux
Fr = Froude number
f = Coriolis parameter
g = Acceleration due to gravity
h = Depth of water
Δh = Change in depth
k = Dimensionless drag coefficient
L = Channel length
P = Power
Q = Flow rate
T = Thrust exerted from a turbine(s) to the fluid
u, v = Depth averaged velocity components
X = Net force between turbine and bypass flows
x, y = Cartesian co-ordinate system
α, β = Velocity coefficients
φ = Tidal phase
γ = Multiplier
Γ = Numerical boundary
η = Efficiency
ρ = Fluid density
τ = Shear stress
ζ = Wave height
ω = Angular frequency of the tide
W = Channel breadth

Subscripts and Superscripts

b = Bypass streamtube
d = Dimensionless drag
h, v = Horizontal and vertical directions
i = Index
n = Normal direction
o = Open ocean boundary
P = Dimensionless power
p = Boundary value external to a finite volume
T = Dimensionless thrust
t = Turbine streamtube
W = Wake
$*$ = Solution at flux interface

Figures

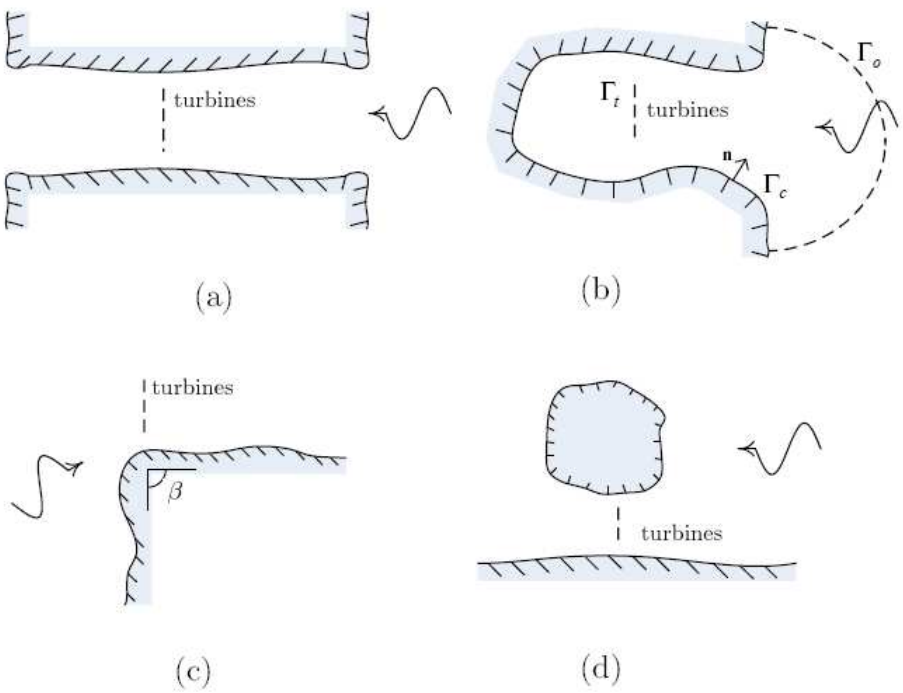

Figure 1: Idealised coastal basins for tidal energy extraction. Fig. 1(b) includes a partitioned boundary Γ, discussed in Section 5.

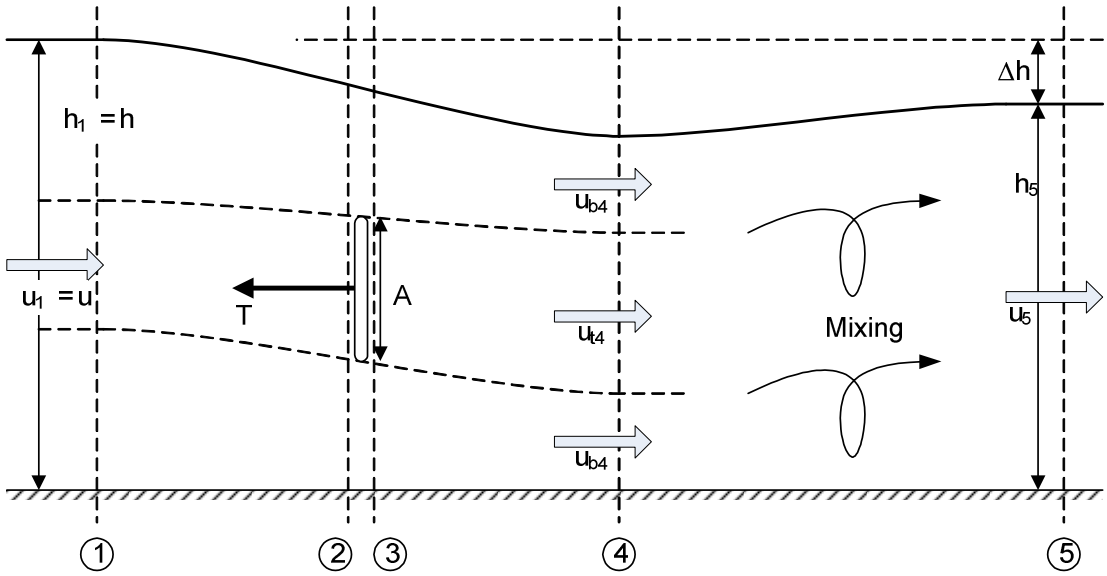

Figure 2: Linear momentum actuator disc theory in an open channel flow. The flow field has a uniform width b, out of the page. Figure taken from [17].

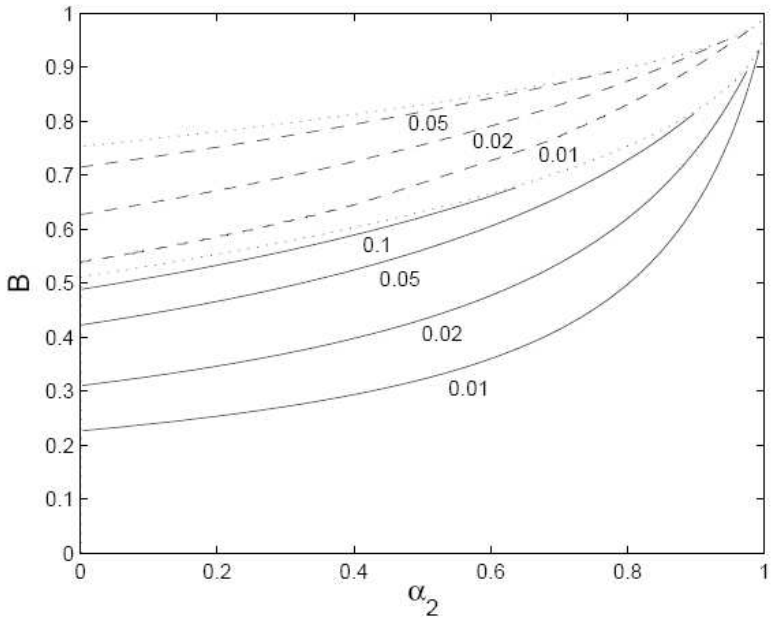

Figure 3: Contours of dimensionless depth change, as a function of turbine velocity coefficient α_2, and blockage ratio B. The dashed lines are for $Fr = 0.05$, the solid lines for $Fr = 0.15$, and the dotted lines represent the cut-off condition at which the bypass flow becomes critical.

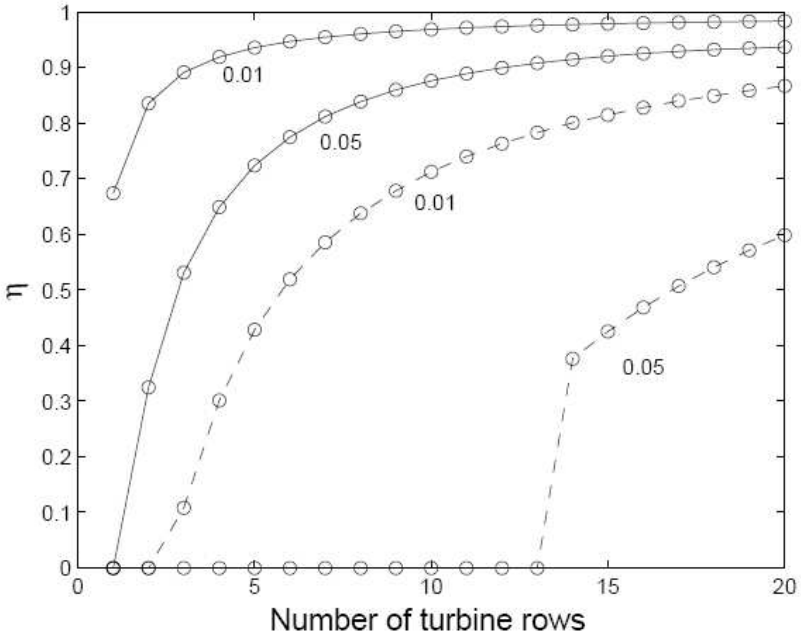

Figure 4: Efficiency as a function of the number of turbine rows, used in series, to extract energy. The initial blockage ratio is 0.4. The total non-dimensional downstream depth change is labelled. The dashed lines are for $Fr = 0.05$ and the solid lines for $Fr = 0.15$. Note in some instances several rows are needed before extraction occurs because, if fewer rows are used, the required depth change across the first row is physically inadmissible.

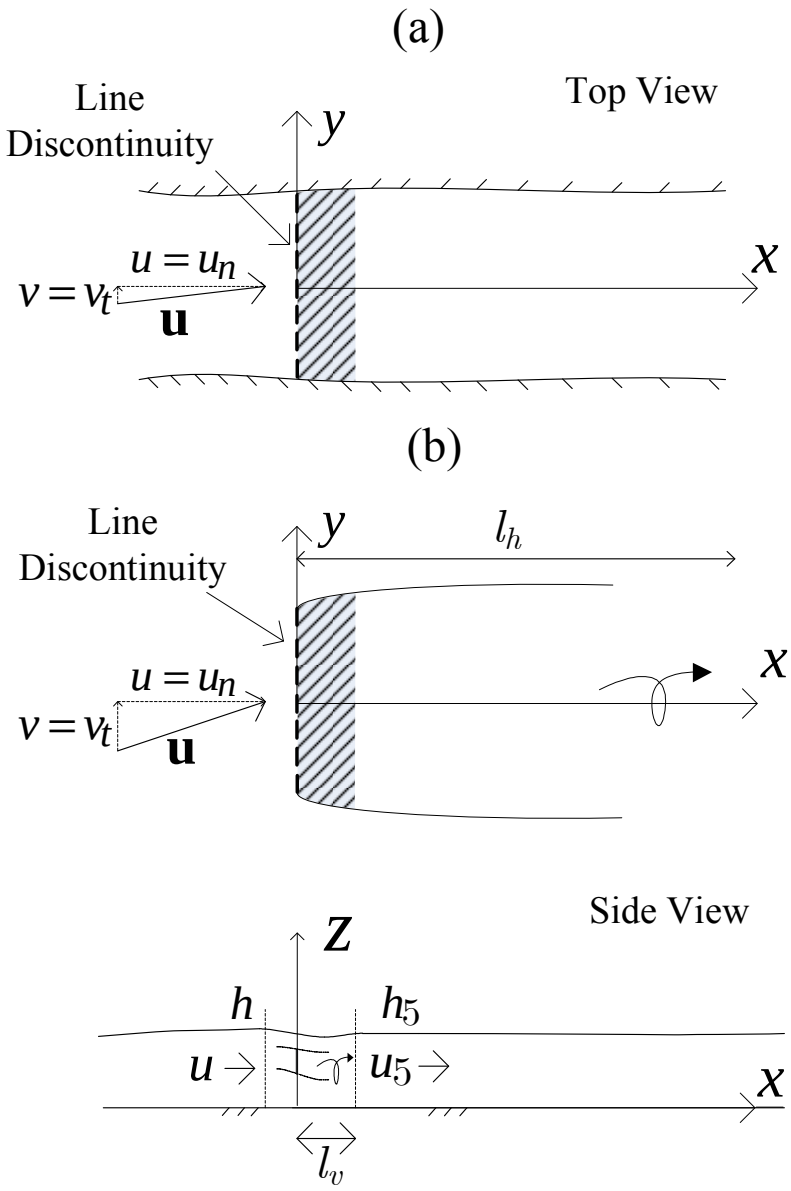

Figure 5: Plan view of a fence of tidal turbines in (a) a confined channel and (b) an unbounded 2D flow.

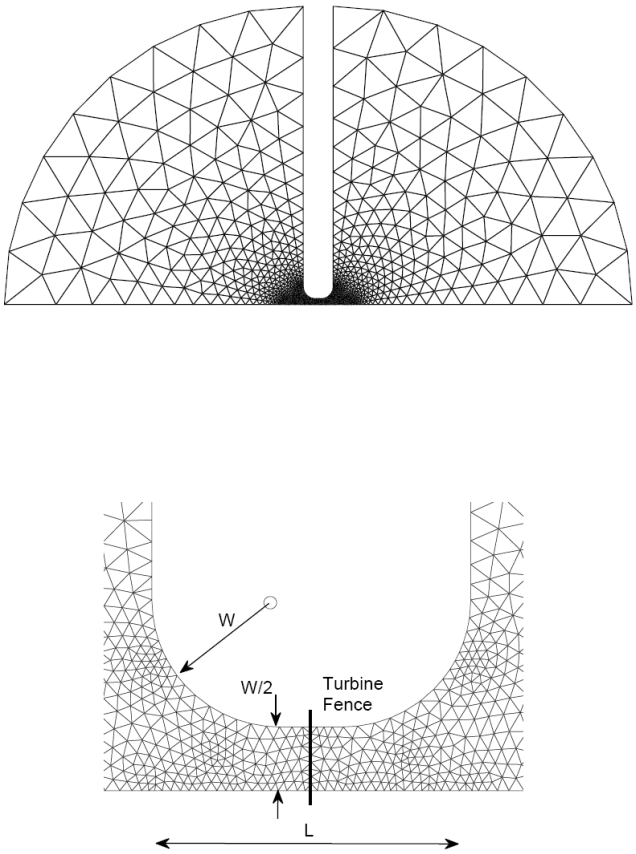

Figure 6: Example numerical mesh and geometry for the simple channel (half mesh only, exploiting axis of symmetry).

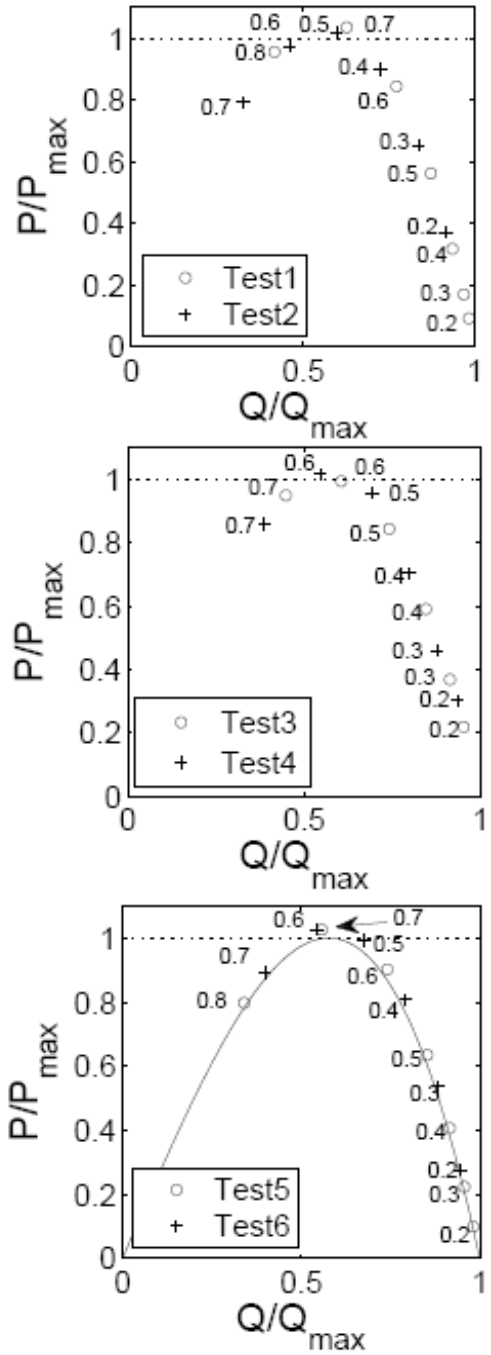

Figure 7: Plot of normalised power against normalised flow rate. The individual points represent the blockage ratio of the tidal fence. The solid line plotted with test 5 and 6 indicates the quasi-steady analytical solution due to [1].

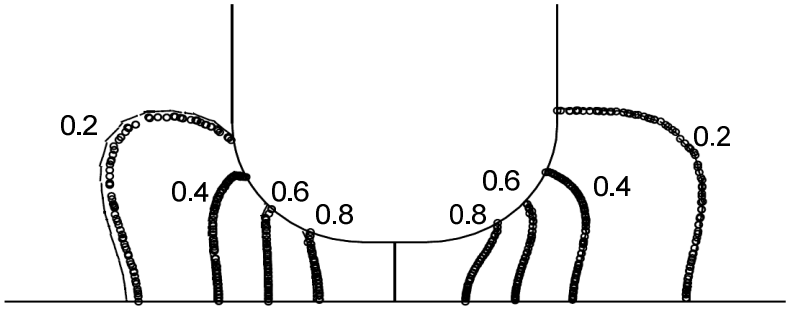

Figure 8: Contour lines of velocity, normalised by maximum velocity, after 9 tidal periods for Test1. The solid lines are calculated for a turbine fence with no blockage ($B = 0$), the circle marker line is calculated for a turbine fence of blockage $B = 0.7$. Note that both lines have considerable overlap.